

Effect of spark plasma sintering (SPS) on the thermoelectric properties of magnesium ferrite

Ryosuke S. S. Maki^{1,2} · Seiji Mitani^{2,3} · Takao Mori^{1,2}

Received: 8 September 2016 / Accepted: 4 December 2016 / Published online: 16 December 2016
© The Author(s) 2016. This article is published with open access at Springerlink.com

Abstract Magnesium ferrite MgFe_2O_4 was synthesized with two different methods, spark plasma sintering (SPS) and conventional solid-state reaction sintering (SSRS), and thermoelectric properties were investigated. SPS processing was found to yield two attractive features: SPS at 900 °C enabled retaining the submicron particle size of 0.3–0.5 μm from ball-milling, leading to lower thermal conductivity, 3 W/mK@300 K. 1200 °C SPS sintering led to the same sample grain size of 1.0–3.0 μm as SSRS, but still exhibited significantly lower thermal conductivity of 4.3 W/mK@300 K compared to the SSRS sample with 14 W/mK@300 K, which exhibited neck formation between particles. Furthermore, while the finer microstructuring led to a reduction in the thermal conductivity, the resistivity of SPS MgFe_2O_4 showed little dependence on the particle size at expected thermoelectric working temperatures above 523 K, which indicates success to some degree of phonon selective scattering due to differences in mean-free-paths of electrons and phonons. As a process, SPS samples are found to exhibit four- to sevenfold enhancement of ZT compared to the conventional SSRS sample. While the maximum ZT in the present samples is relatively low, taking a value of 0.07 for the SPS 1200 °C sintered sample, the processing insights may be utilized for similar systems.

Keywords Thermoelectric properties · Spinel · Magnesium ferrite (MgFe_2O_4) · Spark plasma sintering (SPS) · Induction furnace (IF)

Introduction

Thermoelectric materials have attracted interest because of the potential large benefits of solid-state conversion of waste heat to electricity [1–4]. Some impactful high-temperature thermoelectric applications have recently been reviewed [5]. For very high temperatures, applicable materials will naturally be limited to refractory materials with good heat resistance, like borides [6–8] and oxides [9–12], etc. The material system of spinel-type oxide exists for a wide range of constituent elements, and various chemical and physical properties have been studied [13–17]. Our initial motivation to focus particularly on the spinel-type magnesium ferrites is because its magnetic properties have been extensively studied [13, 14], and we are interested in the link between magnetism (magnetic semiconductors) and thermoelectric properties due to our previous work in chalcopyrite, where thermoelectric enhancement was indicated [18–20]. It is also a system where the crystal structure is well-characterized in a wide temperature range, and a system with good thermal stability and sintering characteristics, and in the present work we tried to learn more about processing effects on its thermoelectric properties.

The performance of thermoelectric materials is gauged by the figure of merit:

$$ZT = \alpha^2 \cdot \sigma \cdot T / \kappa, \quad (1)$$

where T is the temperature, α is the Seebeck coefficient, σ is the electrical conductivity, and κ is the thermal

✉ Takao Mori
MORI.Takao@nims.go.jp

¹ National Institute for Materials Science (NIMS), MANA, Namiki 1-1, Tsukuba 305-0044, Japan

² Graduate School of Pure and Applied Sciences, University of Tsukuba, 1-1-1 Tennodai, Ibaraki 305-8573, Japan

³ National Institute for Materials Science (NIMS), Sengen 1-2-1, Tsukuba 305-0047, Japan

conductivity. The denominator $\alpha^2 \cdot \sigma$ is the power factor. There are some difficulties to straightforwardly obtain high values of ZT because of the typical tradeoff between Seebeck coefficient and electrical conductivity, and conducting electricity well but not heat is also somewhat paradoxical.

In regards to the latter problem, different methods of nanostructuring have been shown to be quite effective to lower the lattice thermal conductivity and enhance ZT [21–28]. Nanostructuring of oxides has been actively carried out [29–31]. Finding ways to enhance the power factor is still a large challenge [32]. Various band engineering methods have been proposed, such as utilization of confinement effects [33], resonance levels [34], modulation doping [35, 36], etc. As a more phenomenological and easily accessible enhancement effect compared to band engineering, large enhancements in the power factor have been reported for nanocomposites [37–41], with mechanisms not fully elucidated. Recently, enhancement has also been proposed for magnetic semiconductors [18–20].

In this work, we have investigated the effect on the thermoelectric properties of magnetic magnesium ferrites synthesized with different conditions to add more insight into this field.

Experiment

In situ reactive synthesis of MgFe_2O_4 was performed using spark plasma sintering (SPS, FUJI DENPA KOKI SPS-1080). The starting materials MgO (99.9%, Wako Pure Chemical Industries Ltd.) and Fe_2O_3 (99.9%, Wako Pure Chemical Industries Ltd.) were mixed with a nominal composition of MgFe_2O_4 using planetary ball-milling with chromium iron media. The powder mixtures were pulverized for 3 h in helium atmosphere. In order to measure thermoelectric properties, samples were prepared by pressing at 60 MPa for 3 min at 900–1200 °C in argon atmosphere using SPS. Prior to the sintering, the powder mixtures were put into graphite dies with diameters of 10 mm, and with graphite foil inserted between the sample and the die/punches. The heating rate for the SPS experiments in the graphite die was limited to 100 °C min^{-1} . The die was wrapped in carbon felt when heating up to 1200 °C. For comparison of the thermoelectric properties of the sample prepared with SPS and standard ceramic procedure, a conventional oxide sample was prepared with solid-state reaction sintering (SSRS) at 1200 °C for 12 h in air using a green pellet uniaxially pressed at 7.4 MPa for 1 min. In addition, we prepared the oxygen defect-rich sample by heating a green pellet set into a carbon crucible at 1200 °C for 12 h with an induction furnace (IF) in order to examine the effect of oxygen vacancies on

thermoelectric properties. Then, the sample was pulverized in an agate mortar and pressed at 80 MPa for 5 min at 900 °C in argon atmosphere with SPS.

The constitution phases in the pulverized samples were analyzed by X-ray powder diffraction measurement with $\text{CuK}\alpha$ radiation (RIGAKU RINT-ULTIMA 3) operated at 40 kV and 40 mA. The detailed crystal structure and site occupancies at cation sites were determined by means of Rietveld refinement using Rietan-FP software [42]. Microstructural observation was carried out by a scanning electrical microscope (JEOL SM-67F, operated at 10 kV). Resistivity and thermoelectric power were measured with a TE measurement system (ULVAC ZEM-2) by using four-probe method and differential method, respectively. In order to determine the thermal conductivity, high-temperature thermal diffusivity coefficient and specific heat were measured by a laser flash method (ULVAC TC-7000) and a differential scanning calorimetry (Rigaku Thermo plus EVO 2), respectively.

Results and discussion

Constitution phase and microstructure

Prior to the Rietveld refinement, constitution phases were identified with ICDD-JCPDS database [PDF 00-036-0398 and 00-035-1393 (ICDD, 1984 and 1983)]. The phase constitutions for each sample are shown in Fig. 1. The XRD patterns reveal that all samples prepared with SPS are constituted of MgFe_2O_4 as the main phase. The sample prepared with SPS at 1200 °C contains minor impurity, $\text{Mg}_{1-x}\text{Fe}_x\text{O}$. In this study, we have induced the excessive oxygen vacancies into MgFe_2O_4 spinel structure with IF in order to clarify its performance as thermoelectric material. The sample prepared with SPS at 900 °C after heating in IF (IF-SPS) mainly contains MgFe_2O_4 phase and quite small impurity content of $\text{Mg}_{1-x}\text{Fe}_x\text{O}$. Figure 2 shows the site occupation at tetragonal A- and octahedral B-site of MgFe_2O_4 refined by Rietveld analysis based on the XRD data. A-site is mainly occupied by Fe^{3+} . Cation distribution at the tetragonal A-site in SPS samples are slightly disordered due to the higher cooling velocities compared to the SSRS sample. These values have relatively good agreement with previous research, which yielded cation distribution for MgFe_2O_4 given by $(\text{Mg}_{0.25} \pm 0.04 \text{Fe}_{0.75} \pm 0.04)[\text{Mg}_{0.75} \pm 0.04 \text{Fe}_{1.25} \pm 0.04]\text{O}_4$ for quenched samples and $(\text{Mg}_{0.12} \pm 0.04 \text{Fe}_{0.88} \pm 0.04)[\text{Mg}_{0.88} \pm 0.04 \text{Fe}_{1.12} \pm 0.04]\text{O}_4$ for slowly cooled samples from Mossbauer studies, respectively [43]. The B-site occupancy ratio of Fe^{3+} to Mg^{2+} is found to be an average 6:4 in this study.

Typically, the thermoelectric performance strongly depends on the particle morphology and density. Here, we

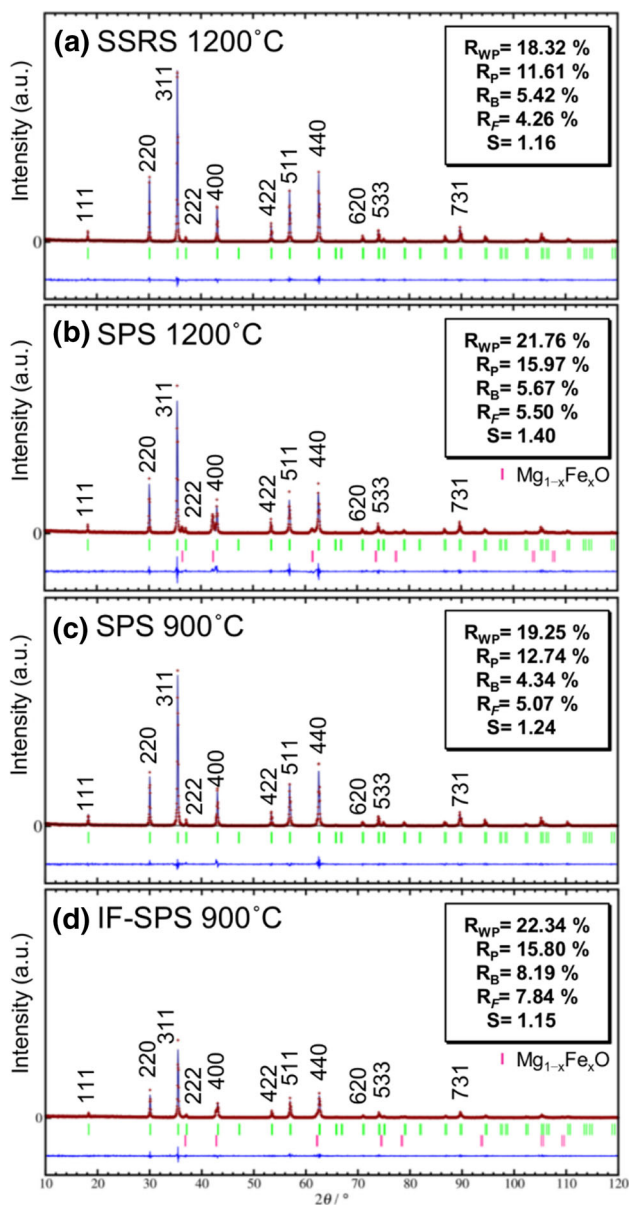


Fig. 1 X-ray diffraction patterns and results of the Rietveld refinement of samples prepared with **a** solid-state reactive sintering (SSRS), spark plasma sintering (SPS) at **b** 1200 °C and **c** 900 °C, and **d** inductive furnace at 1200 °C with SPS treatment at 900 °C (IF-SPS). All peaks are MgFe_2O_4 , with slight impurity of $\text{Mg}_x\text{Fe}_{1-x}\text{O}$ in SPS 1200 °C and IF-SPS 900 °C sample (major peak of $\text{Mg}_x\text{Fe}_{1-x}\text{O}$: $2\theta = 42^\circ$)

compare the microstructures of fracture surfaces of sintered samples. The SEM images for each sample are shown in Fig. 3. The averaged particle size in the samples prepared with (a) SSRS and (b) SPS at 1200 °C is approximately 1.0–3.0 μm ; there are no differences in the particle size. On the other hand, the neck formation between particles is clearly observed only in the SSRS sample. Hence, we consider the contribution of the particle morphology to thermoelectric properties in these samples in the following

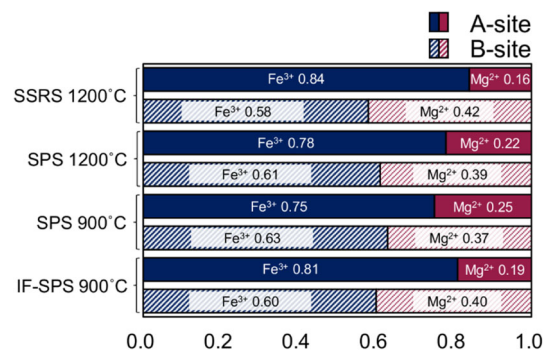


Fig. 2 Cation occupancies at the tetrahedral A-site and octahedral B-site of MgFe_2O_4

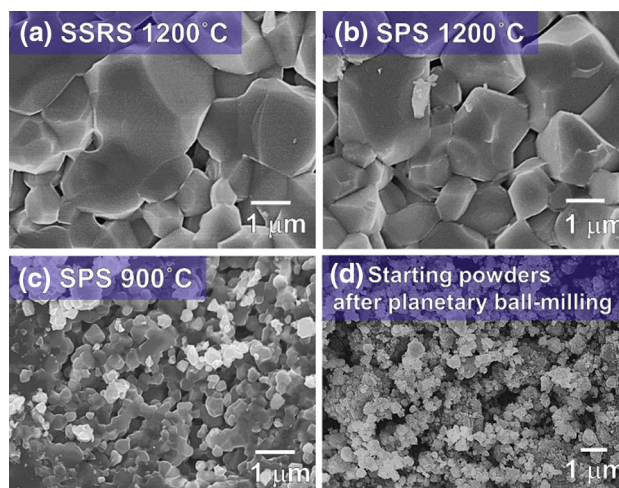
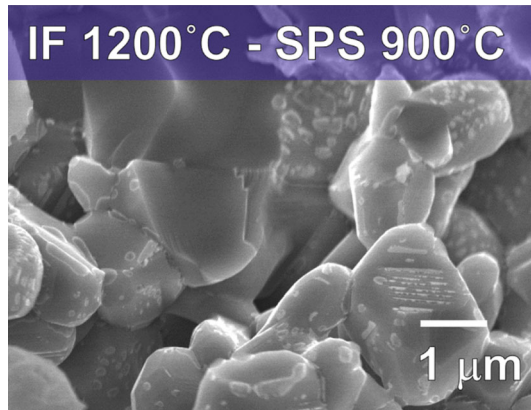


Fig. 3 Microstructural fracture surface of **a** solid-state reactively sintered (SSRS) sample at 1200 °C and spark plasma sintered (SPS) MgFe_2O_4 at **b** 1200 °C and **c** 900 °C. MgO and Fe_2O_3 starting powders after planetary ball-milling are shown in part **(d)**. Particle size of **a** SSRS 1200 °C, **b** SPS 1200 °C, **c** SPS 900, and **d** starting powders are 1.0–3.0, 1.0–3.0, 0.3–0.5, and 0.2–0.5 μm , respectively

section. In the sample prepared with SPS at 900 °C (Fig. 3c), the particle size is approximately 0.3–0.5 μm . This value is similar to that of the starting powder mixture after planetary ball-milling (Fig. 3d), which indicates the effectiveness of the SPS treatment. As shown in our SEM images, the amazing short sintering time with SPS makes it possible to restrict the grain growth while achieving high sample density. Table 1 shows the synthesis conditions, relative densities, particle sizes, refined lattice constants, and detected impurity. The relative densities of the samples prepared with SSRS and SPS are about 90%. The sample prepared with IF-SPS, however, has lower relative density ($\sim 78\%$) compared with that of SSRS and SPS samples. This is attributed to the coarse particles formed during the heating at 1200 °C in IF. The particle size of IF-SPS sample seems to be almost the same with that of SSRS and SPS samples prepared at 1200 °C (Fig. 4).

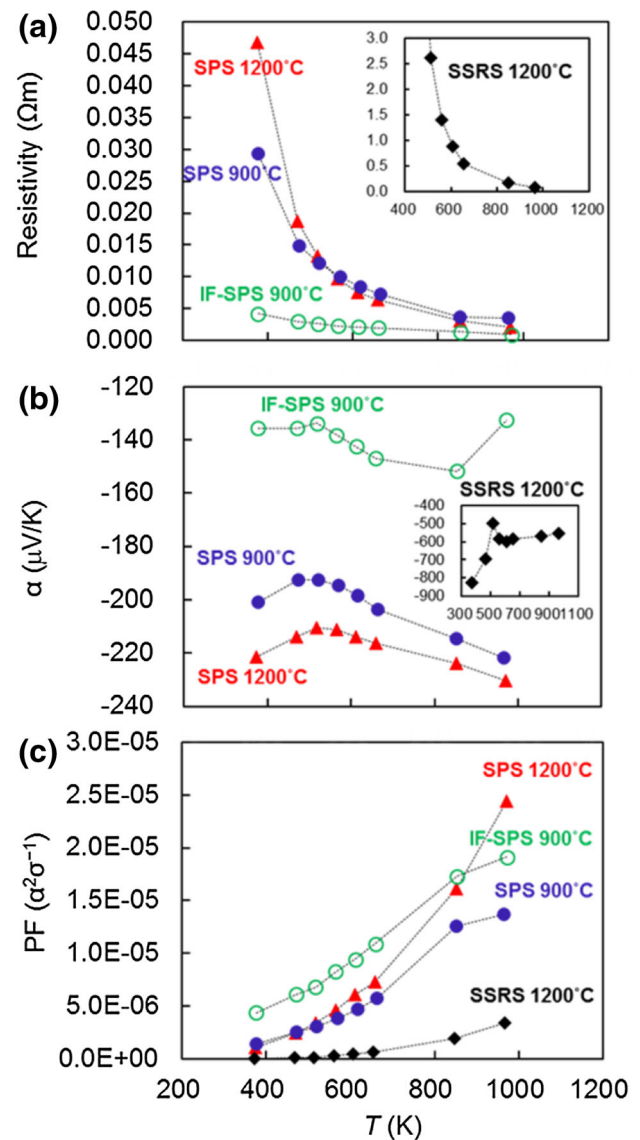
Table 1 Synthesis conditions and sample details

| Procedure | Conditions | Relative density (%) | Particle size (μm) | a (\AA) | Impurity |
|-----------|--------------------|----------------------|---------------------------------|----------------------|---|
| SSRS | 1200 °C 12 h | 90.2 | 1.0–3.0 | 8.387 | – |
| SPS | 1200 °C 3 min | 91.4 | 1.0–3.0 | 8.394 | $\text{Mg}_{0.68}\text{Fe}_{0.32}\text{O}$ |
| | 900 °C 3 min | 87.4 | 0.3–0.5 | 8.390 | – |
| IF + SPS | (IF) 1200 °C 12 h | 77.9 | 1.0–3.0 | 8.394 | $\text{Mg}_{0.93}\text{Fe}_{0.07}\text{O}$ (slight) |
| | (SPS) 900 °C 3 min | | | | |

**Fig. 4** Microstructural fracture surface of spark plasma sintered (SPS) MgFe_2O_4 at 900 °C after heating at 1200 °C in IF (IF-SPS). Averaged grain size is 1.0–3.0 μm

Thermoelectric properties

The temperature dependence of the electrical resistivity is given in Fig. 5a. In the entire temperature range, the resistivity of all samples decreases with increasing temperature, which indicates the typical semiconducting behavior. The samples prepared with SPS exhibit more than two orders of magnitude lower resistivity than that of the sample prepared with SSRS, indicating the significant influence of the SPS process. The SPS sample prepared at 1200 °C exhibits drastically lower resistivity compared to the sample prepared with SSRS despite similar particle sizes, indicating improved, more conducting interfaces at the grain boundaries for the SPS sample. Among the samples prepared with SPS, although the sample prepared at 900 °C shows finer particles (larger amount of grain boundaries) compared with the sample prepared at 1200 °C, the resistivities of both samples are almost the same above 523 K. Considering the differences in thermal conductivity which will be discussed next, this indicates success to some degree of phonon selective scattering due to differences in mean-free-paths of electrons and phonons. Namely, the differences in particle size of 1.0–3.0 and

**Fig. 5** Temperature dependence of **a** resistivity, **b** Seebeck coefficient and **c** power factor (PF) of MgFe_2O_4 prepared with SSRS at 1200 °C (diamonds), SPS at 1200 °C (triangles) and 900 °C (filled circles), and IF-SPS at 900 °C (open circles). The dotted lines are guides to the eye

0.3–0.5 μm have a larger effect on phonons compared to electrons, which assumedly have smaller mean-free-paths. Furthermore, in general, grain boundary scattering has larger effect on the electrical conductivity at lower temperatures [29], which is consistent with what is observed.

In the IF-SPS sample, the resistivity is an order of magnitude lower than that of the SPS sample at 373 K. The resistivities of all samples converge with elevating temperature. In this study, the IF-SPS sample, which contains significant oxygen defects, exhibits the lowest resistivity in spite of its low relative density. In ferrite, the electrical resistivity is due to the electron hopping $\text{Fe}^{2+} \leftrightarrow \text{Fe}^{3+}$ of the spinel structure; high content of Fe^{2+} ions is responsible for low resistivity [44]. In addition, Nozaki et al. reported that the electrical and thermal conductivity of spinel structure could be controlled separately by changing the cation distribution of the tetrahedral A- and octahedral B-site, respectively [45]. In this research, the inducing of excess oxygen vacancies into the spinel structure appears to cause the valence modification from Fe^{3+} to Fe^{2+} , mainly at A-site due to site-preference of the cation [46], which leads to the enhancement of the electrical conductivity.

The temperature dependence of the Seebeck coefficients is given in Fig. 5b. All samples exhibit n-type behavior. Based on the dependence of the Seebeck coefficient on the carrier concentration, the SSRS sample exhibits the highest value, conceivably due to the high resistivity as shown in Fig. 5a. Among the samples prepared with SPS, the sample prepared at 1200 °C exhibits a slightly larger Seebeck coefficient than that of the sample prepared at 900 °C. The IF-SPS sample exhibits the minimum value, which corresponds to its high electrical conductivity indicated to originate from significant oxygen defects, as discussed above. The Seebeck coefficients of all samples decrease from 373 to 523 K, but suddenly exhibit a change in their temperature dependence at around 523 K, corresponding to the magnetic phase transition between the ferrimagnetic phase and paramagnetic phase (Curie point: T_{Curie}). The Seebeck coefficient increases above the T_{Curie} averaged $-20 \mu\text{V/K}$ among the samples prepared with SPS. This enhancement of Seebeck coefficient due to the spin entropy from the varying Fe^{2+} and Fe^{3+} cations in the paramagnetic region was experimentally and mathematically explained by Nozaki et al. [45]. This is similar to the mechanism of enhancement found in sodium cobaltite [9].

Based on an empirical equation of MgFe_2O_4 with the temperature of equilibration reported by Harrison and Putnis [47], the calculated T_{Curie} is given as 549 and 576 K on the basis of our sintering temperature of 1200 and 900 °C, respectively: $T_{\text{Curie}} = 489.186 - 0.296T + 0.00009875T^2$, where T is equilibration temperature. In comparison to the value calculated with sintering

temperature in the case of the SPS samples, T_{Curie} obtained from temperature dependence change in the Seebeck coefficient seems to be lower and the graph peak indicating T_{Curie} became broader than SSRS sample, especially in the IF-SPS sample which includes excessive oxygen defects, and there appears to be no difference of T_{Curie} between SPS samples. Harrison and Putnis reported the strong dependence of T_{Curie} of MgFe_2O_4 on the thermal treatment, stoichiometry and intracrystalline distribution of Fe^{3+} and Mg^{2+} cations using measurements of alternating-field magnetic susceptibility of samples quenched directly from furnace into water [47]. However, the relationship between T_{Curie} and expected defects formed by quenching was not pointed out. This process might lead to valence modification of the cations. We find that it is indicated that the obtained T_{Curie} of spinel structure appears to depend on the amount of defects, namely oxygen vacancies, induced by SPS process. As noted above, the samples prepared with SPS at 1200 and 900 °C clearly indicate the maximum peak value of Seebeck coefficient at 523 K. The IF-SPS sample, which is indicated to include excessive defects as discussed above from the resistivity results (Fig. 5a), exhibits the broadened peak shift of T_{Curie} to lower temperature.

The temperature dependence of the power factor is given in Fig. 5c. In the temperature range of 373–853 K, the IF-SPS sample exhibits the highest power factor because of its low resistivity. At 973 K, the maximum power factor is obtained for the sample prepared with SPS at 1200 °C.

The temperature dependence of the thermal conductivity is given in Fig. 6. The thermal conductivity of the sample prepared with SSRS is the highest value below 673 K. Among the SPS samples, the thermal conductivity of the sample prepared at 900 °C is about a half of that of the sample prepared at 1200 °C. It is indicated that fine grains effectively scatter the phonons at the grain boundaries,

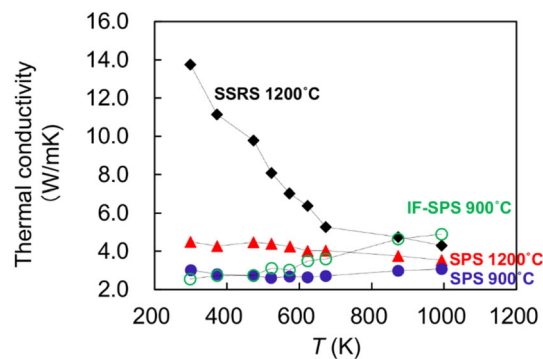


Fig. 6 Temperature dependence of thermal conductivity of MgFe_2O_4 prepared with SSRS at 1200 °C (diamonds), SPS at 1200 °C (triangles) and 900 °C (filled circles), and IF-SPS at 900 °C (open circles). The dotted lines are guides to the eye

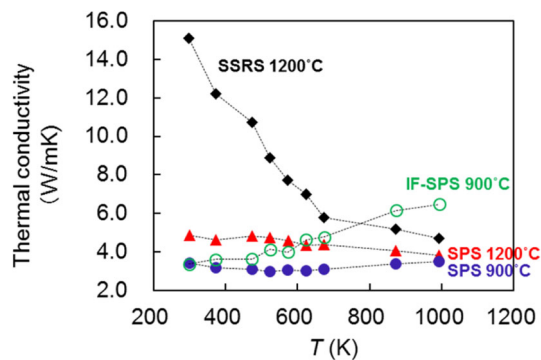


Fig. 7 Thermal conductivity values corrected for porosity of MgFe_2O_4 prepared with SSRS at 1200 °C (diamonds), SPS at 1200 °C (triangles) and 900 °C (filled circles), and IF-SPS at 900 °C (open circles). The corrected thermal conductivity is given as $\kappa/(1 - P)$, where κ and P are the measured thermal conductivity and the porosity. The dotted lines are guides to the eye

leading to lower thermal conductivity. In contrast, the thermal conductivity of the IF-SPS sample increases with elevating temperature and becomes the highest value at 993 K. Although the particle size in the samples prepared at 1200 °C with SSRS and SPS is almost same, SSRS sample exhibits much higher thermal conductivity due to the neck formation between particles, which indicates the effectiveness of the SPS treatment. In addition to this, the induced oxygen vacancies possibly led to additional phonon scattering and increased electron concentration as well. In the entire temperature range, the SPS samples, especially the IF-SPS sample, achieve much higher electrical conductivity and lower thermal conductivity compared to the sample prepared with conventional SSRS method. In this research, the relative density of the samples varies from 78 to 91%. This porosity variation can significantly compromise the comparison of the thermoelectric properties of these samples. Therefore, the thermal conductivity was corrected for porosity by calculating the thermal conductivity at the theoretical density, κ_0 , using the following equation:

$$\kappa = \kappa_0(1 - P), \quad (2)$$

where κ and P are the measured thermal conductivity and the porosity, respectively [48, 49]. The thermal conductivity values corrected for porosity were plotted in Fig. 7. The corrected thermal conductivity, κ_0 , indicated almost the same tendency shown in Fig. 6.

In this research, the influence of the oxygen-defect on the thermoelectric properties of magnesium ferrite was discussed. However, to quantitatively determine the effects of oxygen vacancy with the present research is difficult because it is impossible to detect the oxygen vacancies and the small difference between the atomic scattering factors of Fe^{2+} and Fe^{3+} ions by conventional XRD analysis.

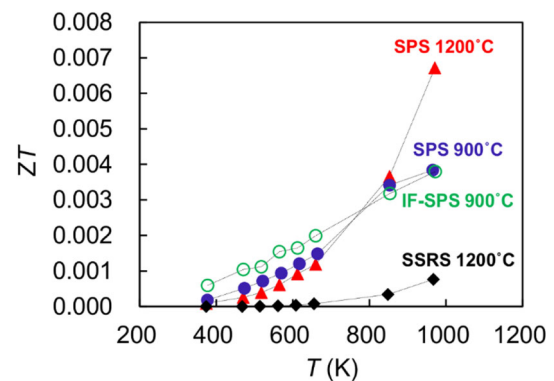


Fig. 8 Temperature dependence of figure of merit ZT of MgFe_2O_4 prepared with SSRS at 1200 °C (diamonds), SPS at 1200 °C (triangles) and 900 °C (filled circles), and IF-SPS at 900 °C (open circles). The dotted lines are guides to the eye

Moreover, the significant cation disorder of MgFe_2O_4 at high temperature (above 581 °C determined from in situ synchrotron X-ray powder-diffraction data [50]) also makes it difficult to determine the accurate crystal structure of oxygen-deficient MgFe_2O_4 . To clarify in detail the attractiveness of the SPS treatment for spinel-type thermoelectric materials, further detailed research for quantitative analysis on the effect of oxygen-defects on the thermoelectric properties is required.

The temperature dependence of the dimensionless figure of merit, ZT , is given in Fig. 8. As a result of the thermoelectric properties of oxygen-deficient MgFe_2O_4 , the IF-SPS sample including excessive oxygen vacancies exhibits the highest ZT value at 373–673 K. In the temperature range of 873–993 K, the SPS sample sintered at 1200 °C exhibits the highest ZT value. Although the absolute maximum value is not high with $ZT = 0.007$, the SPS samples exhibit a four- to sevenfold enhancement compared to the SSRS sample because of lower electrical resistivities and thermal conductivities.

Conclusion

Magnesium ferrite MgFe_2O_4 was synthesized with two different methods, spark plasma sintering (SPS) and conventional solid-state reaction sintering (SSRS), and the thermoelectric properties investigated. SPS processing was found to yield two attractive features. SPS at 900 °C enabled retaining the submicron particle size of 0.3–0.5 μm from ball-milling, leading to lower thermal conductivity. While 1200 °C SPS sintering led to the same grain size of 1.0–3.0 μm as SSRS, it still exhibited lower thermal conductivity due to the neck formation between particles with SSRS. Furthermore, the resistivity of SPS MgFe_2O_4 showed little dependence on the particle size at

expected working temperatures above 523 K, indicating success to some degree of phonon selective scattering due to differences in mean-free-paths of electrons and phonons. An oxygen defect-rich sample was also prepared with an induction furnace and SPS, with large reduction of resistivity and Seebeck coefficient. The kink in the temperature dependence of the Seebeck coefficient which is representative of T_{Curie} is sizably reduced, indicating effects from oxygen defects. As a process, the SPS samples are found to exhibit four- to sevenfold enhancement of ZT compared to the conventional SSRS. While the maximum ZT in the present samples is relatively low, taking a value of 0.07 for the SPS 1200 °C sintered sample, the processing insights may be utilized for similar systems.

Acknowledgements TM and SM thank JST, CREST for support.

Open Access This article is distributed under the terms of the Creative Commons Attribution 4.0 International License (<http://creativecommons.org/licenses/by/4.0/>), which permits unrestricted use, distribution, and reproduction in any medium, provided you give appropriate credit to the original author(s) and the source, provide a link to the Creative Commons license, and indicate if changes were made.

References

- Koumoto, K., Mori, T.: Thermoelectric nanomaterials; materials design and applications, Springer series in materials science, vol. 182. Springer, Heidelberg (2013)
- Rome, D.M.: Modules, systems, and applications in thermoelectrics, vol. 14. CRC Press, London (2012)
- Nolas, G.S., Sharp, J., Goldsmid, J.: Thermoelectrics, basic principles and new materials developments, Springer series in materials science, vol. 45. Springer, Heidelberg (2001)
- Dames, C.: Cost optimization of thermoelectric materials for power generation: the case for ZT at (almost) any cost. *Scripta Mater.* **111**, 16–22 (2016)
- Mori, T.: Perspectives of high-temperature thermoelectric applications and p-type and n-type aluminoborides. *JOM Press* (2016). doi:10.1007/s11837-016-2069-9
- Mori, T., Nishimura, T.: Thermoelectric properties of homologous p- and n-type boron-rich borides. *J. Solid State Chem.* **179**, 2908–2915 (2006)
- Maruyama, S., Miyazaki, Y., Hayashi, K., Kajitani, T., Mori, T.: Excellent p-n control in a high temperature thermoelectric boride. *Appl. Phys. Lett.* **101**, 152101 (2012)
- Mori, T., Berthebaud, D., Nishimura, T., Nomura, A., Shishido, T., Nakajima, K.: Effect of Zn doping on improving crystal quality and thermoelectric properties of borosilicides. *Dalton Trans.* **39**, 1027–1030 (2010)
- Terasaki, I.: Layered cobalt oxides: correlated electrons for thermoelectrics. In: Koumoto, K., Mori, T. (eds.) Thermoelectric nanomaterials; materials design and applications, Springer series in materials science. vol. 182, pp. 51–70. Springer, Heidelberg (2013)
- Terasaki, I., Okazaki, R., Mondal, P.S., Hsieh, Y.C.: Trials for oxide photo-thermoelectrics. *Mater. Renew. Sustain. Energy* **3**, 29 (2014)
- Delacotte, C., Hébert, S., Maki, R., Mori, T., Pelloquin, D.: Impact of densification on microstructure and transport properties of CaFe_5O_7 . *Solid State Sci.* **54**, 54–58 (2016)
- Terasaki, I., Okazaki, R., Ohta, H.: Search for non-equilibrium thermoelectrics. *Scripta Mat.* **111**, 23–28 (2016)
- Liu, C., Zou, B., Rondinone, A.J., Zhang, Z.J.: Chemical control of superparamagnetic properties of magnesium and cobalt spinel ferrite nanoparticles through atomic level magnetic couplings. *J. Am. Chem. Soc.* **122**, 6263 (2000)
- Zhang, C.L., Yeo, S., Horibe, Y., Choi, Y.J., Guha, S., Croft, M., Cheong, S.-W., Mori, S.: Coercivity and nanostructure in magnetic spinel $\text{Mg}(\text{Mn}, \text{Fe})_2\text{O}_4$. *Appl. Phys. Lett.* **90**(13), 3123 (2007)
- Fujishiro, Y., Hamamoto, K., Shiono, O., Katayama, S., Awano, M.: Synthesis and thermoelectric characterization of polycrystalline $\text{Ni}_{1-x}\text{Ca}_x\text{Co}_2\text{O}_4$ ($x = 0 - 0.05$) spinel materials. *J. Mater. Sci. Mater. El.* **15**, 769–773 (2004)
- Watanabe, N., Nakayama, H., Fukao, F., Munakata, F.: Effects of metal substitution on the electric and thermoelectric properties in $(\text{Ni}_{1-x}\text{M}_x)\text{Mn}_2\text{O}_4$ ($\text{M}=\text{Zn}$ and Mg). *Thermochim. Acta* **532**, 56–59 (2012)
- Nakamura, Y., Kakemoto, H., Nishiyama, S., Irie, H.: Synthesis and thermoelectric properties of the novel A-site deficient $\text{Zn}_{0.5}\text{Rh}_2\text{O}_4$ compound. *J. Solid State Chem.* **192**, 23–27 (2012)
- Tsujii, N., Mori, T.: High thermoelectric power factor in a carrier-doped magnetic semiconductor CuFeS_2 . *Appl. Phys. Express* **6**, 043001 (2013)
- Tsujii, N., Mori, T., Isoda, Y.: Phase stability and thermoelectric properties of CuFeS_2 -based magnetic semiconductor. *J. Electron. Mater.* **43**, 2371–2375 (2014)
- Ang, R., Khan, A.U., Tsujii, N., Takai, K., Nakamura, R., Mori, T.: Thermoelectricity generation and electron-magnon scattering in a natural chalcopyrite mineral from a deep-sea hydrothermal vent. *Angew. Chem. Int. Ed.* **54**, 12909–12913 (2015)
- Koumoto, K., Shimohigoshi, M., Takeda, S., Yanagida, H.: Thermoelectric energy conversion by porous SiC ceramics. *J. Mater. Sci. Lett.* **6**, 1453–1455 (1987)
- Hsu, K.F., Loo, S., Guo, F., Chen, W., Dyck, J.S., Uher, C., Hogan, T., Polychroniadis, E.K., Kanatzidis, M.G.: Cubic $\text{AgPb}_m\text{SbTe}_{2+m}$: bulk thermoelectric materials with high figure of merit. *Science* **303**, 818–821 (2004)
- Zhao, X.B., Ji, X.H., Zhang, Y.H., Zhu, T.J., Tu, J.P., Zhang, X.B.: Bismuth telluride nanotubes and the effects on the thermoelectric properties of nanotube-containing nanocomposites. *Appl. Phys. Lett.* **86**, 06211 (2005)
- Poudel, B., Hao, Q., Ma, Y., Lan, Y.C., Minnich, A., Yu, B., Yan, X., Wang, D.Z., Muto, A., Vashaee, D., Chen, X.Y., Liu, J.M., Dresselhaus, M.S., Chen, G., Ren, Z.F.: High-thermoelectric performance of nanostructured bismuth antimony telluride bulk alloys. *Science* **320**, 634–638 (2008)
- Grasso, S., Tsujii, N., Jiang, Q., Khaliq, J., Maruyama, S., Miranda, M., Simpson, K., Mori, T., Reece, M.J.: Ultra low thermal conductivity of disordered layered p-type bismuth telluride. *J. Mater. Chem. C* **1**, 2362–2367 (2013)
- Rogl, G., Setman, D., Schaffer, E., Horky, J., Kerber, M., Zehetbauer, M., Falmbigl, M., Rogl, P., Royanian, E., Bauer, E.: High-pressure torsion, a new processing route for thermoelectrics of high ZT s by means of severe plastic deformation. *Acta Mater.* **60**, 2146–2157 (2012)
- Nethravathi, C., Rajamathi, C.R., Rajamathi, M., Maki, R., Mori, T., Golberg, D., Bando, Y.: Synthesis and thermoelectric behaviour of copper telluride nanosheets. *J. Mat. Chem. A* **2**, 985–990 (2014)
- Khan, A.U., Kobayashi, K., Tang, D., Yamauchi, Y., Hasegawa, K., Mitome, M., Xue, Y., Jiang, B., Tsuchiya, K., Golberg, D., Bando, Y., Mori, T.: Nano-micro-porous skutterudites with 100%

- enhancement in ZT for high performance thermoelectricity. *Nano Energy* **31**, 152 (2017)
29. Kinemuchi, Y., Nakano, H., Mikami, M., Kobayashi, K., Watari, K., Hotta, Y.: *J. Appl. Phys.* **108**, 053721 (2010)
 30. Azough, F., Kepaptsoglou, D., Ramasse, Q.M., Schaffer, B., Freer, R.: On the Origin of Nanocheesboard Superlattices in A-Site-Deficient Ca-Stabilized $\text{Nd}_{2/3}\text{TiO}_3$. *Chem. Mater.* **27**, 497 (2015)
 31. Weidenkaff, A., Robert, R., Aguirre, M.H., Bocher, L., Schlapbach, L.: Nanostructured thermoelectric oxides with low thermal conductivity. *Phys. Stat. Sol. (RRL)* **1**, 247 (2007)
 32. Liu, W., Kim, H.S., Jie, Q., Ren, Z.: Importance of high power factor in thermoelectric materials for power generation application: a perspective. *Scripta Mat.* **111**, 3–9 (2016)
 33. Hicks, L.D., Dresselhaus, M.S.: Effect of quantum-well Structures on the thermoelectric figure of merit. *Phys. Rev. B* **47**, 12727 (1994)
 34. Heremans, J.P., Jovovic, V., Toberer, E.S., Saramat, A., Kurosaki, K., Charoenphakdee, A., Yamanaka, S., Snyder, G.J.: Enhancement of thermoelectric efficiency in PbTe by distortion of the electronic density of states. *Science* **321**, 554–557 (2008)
 35. Zebarjadi, M., Joshi, G., Zhu, G.H., Yu, B., Minnich, A.J., Lan, Y.C., Wang, X.W., Dresselhaus, M.S., Ren, Z.F., Chen, G.: Power factor enhancement by modulation doping in bulk nanocomposites. *Nano Lett.* **11**, 2225–2230 (2011)
 36. Yu, B., Zebarjadi, M., Wang, H., Lukas, K., Wang, H., Wang, D., Opeil, C., Dresselhaus, M.S., Chen, G., Ren, Z.F.: Enhancement of thermoelectric properties by modulation-doping in silicon germanium alloy nanocomposites. *Nano Lett.* **12**, 2077–2082 (2012)
 37. Goto, T.: *Kinzoku*. **68**, 1086–1092 (1998) (in Japanese)
 38. Mori, T., Nishimura, T., Yamaura, K., Takayama-Muromachi, E.: High temperature thermoelectric properties of a homologous series of n-type boron icosahedra compounds: a possible counterpart to p-type boron carbide. *J. Appl. Phys.* **101**, 093714 (2007)
 39. Prytuliak, A., Maruyama, S., Mori, T.: Anomalous effect of vanadium boride seeding on thermoelectric properties of $\text{YB}_{22}\text{C}_2\text{N}$. *Mat. Res. Bull.* **48**, 1972–1977 (2013)
 40. Bing, F., Martin, H.P., Michaelis, A.: In Situ preparation and thermoelectric properties of $\text{B4C}_{1-x}\text{-TiB}_2$ composites. *J. Electron. Mater.* **42**, 2314–2319 (2013)
 41. Mori, T., Hara, T.: Hybrid effect to possibly overcome the trade-off between Seebeck coefficient and electrical conductivity. *Scripta Mater.* **111**, 44–48 (2016)
 42. Izumi, F., Momma, K.: Three-dimensional visualization in powder diffraction. *Solid State Phenom.* **130**, 15–20 (2007)
 43. Sawatzky, G.A., Woude, F.V.D., Morrish, A.H.: Mössbauer study of several ferrimagnetic spinels. *Phys. Rev.* **187**, 747–757 (1969)
 44. Rane, K.S., Verenkar, V.M.S., Sawant, P.Y.: Dielectric behaviour of MgFe_2O_4 prepared from chemically beneficiated iron ore rejects. *Bull. Mater. Sci.* **24**, 323–330 (2001)
 45. Nozaki, T., Hayashi, K., Miyazaki, Y., Kajitani, T.: Cation distribution dependence on thermoelectric properties of doped spinel $\text{M}_{0.6}\text{Fe}_{2.4}\text{O}_4$. *Mater. Trans.* **53**, 1164–1168 (2012)
 46. Dunitz, J.D., Orgel, L.E.: Advanced in inorganic chemistry and radiochemistry. In: Emeleus, H.J., Sharpe, A.G. (eds.) *Stereochemistry of Ionic Solids*, vol. 2. Academic Press Inc., New York (1960)
 47. Harrison, R.J., Putnis, A.: Determination of the mechanism of cation ordering in magnesioferrite (MgFe_2O_4) from the time- and temperature-dependence of magnetic susceptibility. *Phys. Chem. Minerals* **26**, 322–332 (1999)
 48. Francl, J., Kingery, W.D.: Thermal conductivity: IX, experimental investigation of effect of porosity on thermal conductivity. *J. Am. Ceram. Sci.* **37**, 99–107 (1954)
 49. Nozaki, T., Hayashi, K., Kajitani, T.: Mn-substitution effect on thermal conductivity of delafossite-type oxide CuFeO_2 . *J. Electron. Mater.* **39**, 1798–1802 (2010)
 50. Antao, S.M., Hassan, I., Parise, J.B.: Cation ordering in magnesioferrite, MgFe_2O_4 , to 982 °C using in situ synchrotron X-ray powder diffraction. *Am. Mineral.* **90**, 219–228 (2005)